Science of the Total Environment 755 (2021) 143556

Contents lists available at ScienceDirect

Science of the Total Environment

journal homepage: www.elsevier.com/locate/scitotenv

# Study of the photoinduced transformations of maprotiline in river water using liquid chromatography high-resolution mass spectrometry

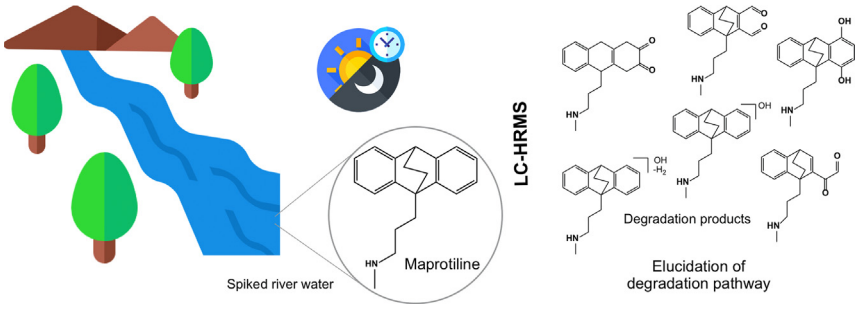
Nuno P.F. Gonçalves [a], Zsuzsanna Varga [b], Stéphane Bouchonnet [b], Valeria Dulio [c], Nikiforos Alygizakis [e,f], Federica Dal Bello [d], Claudio Medana [d], Paola Calza [a,*]

[a] Department of Chemistry, University of Turin, Torino, Italy
[b] Laboratoire de Chimie Moléculaire - CNRS/Ecole Polytechnique, Institut Polytechnique de Paris, 91128 Palaiseau, France
[c] INERIS, National Institute for Environment and Industrial Risks, Verneuil en Halatte, France
[d] Department of Molecular Biotechnology and Health Sciences, University of Turin, Torino, Italy
[e] Laboratory of Analytical Chemistry, Department of Chemistry, University of Athens, Panepistimiopolis Zografou, 15771 Athens, Greece
[f] Environmental Institute, Okružná 784/42, 97241 Koš, Slovak Republic

## HIGHLIGHTS

- The environmental fate of maprotiline in spiked river water was investigated.
- Main degradation products result from the drug hydroxylation in different positions.
- Degradation mechanism has been proposed based on transformation photoproducts structures.
- Maprotiline TPs suggests lower toxicity than the parent compound.

## GRAPHICAL ABSTRACT




## ARTICLE INFO

*Article history:*
Received 6 August 2020
Received in revised form 26 October 2020
Accepted 3 November 2020
Available online 6 November 2020

Editor: Dimitra A. Lambropoulou

*Keywords:*
Contaminants of emerging concern
Maprotiline
Structural elucidation
Degradation pathway
Environmental fate
HRMS

## ABSTRACT

Maprotiline was identified as a compound of potential interest further to a suspect screening test carried out for a list of more than 40,000 substances based on specific occurrence, hazard and risk indicators. Despite the high frequency of appearance of this drug in wastewater treatment stations, his environmental fate is still unknown. Herein, we investigated for the first time the maprotiline degradation pathways in river water spiked with the drug at a concentration close to those detected in natural waters. Preliminary photocatalytic experiments in ultrapure water produced 32 transformation products (TPs) resulted mainly from the multiple hydroxylation/oxidation in different positions of the drug molecule. From the river water experiments, 12 TPs were formed by photolysis matching with those observed in ultrapure water experiments, and 2 were also formed resulted from biotic degradation. Employing HPLC-HRMS, we were able to elucidate the chemical structures of TPs and assess the overall degradation mechanism. Preliminary bioassays suggested lower toxicity of TPs relatively to the parent compound.
© 2020 The Authors. Published by Elsevier B.V. This is an open access article under the CC BY-NC-ND license (http://creativecommons.org/licenses/by-nc-nd/4.0/).

## 1. Introduction

The scientific progress observed in the last few decades had a remarkable impact on modern human lifestyle. The development of countless chemical substances part of our daily routine activities is now severely affecting the quality of water resources. The widespread

* Corresponding author.
*E-mail address:* paola.calza@unito.it (P. Calza).

https://doi.org/10.1016/j.scitotenv.2020.143556
0048-9697/© 2020 The Authors. Published by Elsevier B.V. This is an open access article under the CC BY-NC-ND license (http://creativecommons.org/licenses/by-nc-nd/4.0/).

presence of contaminants of emerging concern (CECs) is a major threat to aquatic ecosystems worldwide (UNESCO World Water Assessment Programme, 2019). According to NORMAN network ("NORMAN Databases"), a CEC is defined as "a substance currently not included in routine environmental monitoring programs that may be a candidate for future legislation due to its adverse effects and/or persistency". These substances are not necessarily new, most of them are "emerging" as result of the improvement in analytical techniques that recently allowed to detect and track trace concentrations in aquatic media (Hollender et al., 2019; Nawaz and Sengupta, 2018). Their "concern" rises from the scarce information about their environmental fate, their hazards to human health and ecosystems, the degradation pathway and toxicity of their degradation products. The presence of a large number of contaminants coupled with the continuous improvement capability to detect new pollutants make CECs a complex challenge for regulatory agencies (Brack et al., 2019; Sauvé and Desrosiers, 2014).

Pharmaceuticals have emerged in the past few decades as the CECs epicenter (aus der Beek et al., 2016; Ebele et al., 2017; Lai et al., 2016; Vandermeersch et al., 2015). The increasing number of new medicines together with their extensive use, persistence and high biological activity enlarged drastically their environmental impact (Küster and Adler, 2014). Pharmaceuticals reach the environment mainly by excretions and erroneous disposal in the domestic sewer, hospital effluents and animal/fish farming. They include antibiotics, hormones, birth control pills, antidiabetics, beta-blockers, lipid regulators, impotence drugs, painkillers, tranquilizers, antidepressants and other medicines. Furthermore, the actual wastewater treatment facilities are not specifically designed to remove organic pollutants, thereby allowing their constant release into the environment (Gogoi et al., 2018; Krzeminski et al., 2019; UNESCO and HELCOM, 2017).

Antidepressants are among the most prescribed pharmaceuticals in developed countries (Abbing-Karahagopian et al., 2014; Pratt et al., 2017), associated with psychiatric disorders also in the youngest generation. The consequent appearance of these complex mixtures in water stream impacts animals living in the aquatic environment (Ford and Herrera, 2019). Recent studies linked antidepressants exposure to different disorders in the aquatic biota (David et al., 2018; Sehonova et al., 2018). For example, oxazepam was reported to affect the activity, sociality and feeding rate of *Perca fluviatilis* even at the concentration level detected in wastewater treatment influents/effluents (Brodin et al., 2013). Such behavioral changes may have ecological and evolutionary consequences.

Maprotiline is a tetracyclic antidepressant drug approved in many countries, with a daily usual dosage of 150 to 225 mg used to treat depression associated with agitation or anxiety (Aronson, 2016). As a consequence of its wrong disposal and excretion in its unmetabolized form (3–4%), (Breyer-Pfaff et al., 1985), like many other drugs, maprotiline drug has been reported in influent and effluent of wastewater treatment plants as well as in surface waters, usually at ng/L up to few μg $L^{-1}$ concentration (Loos et al., 2013; Sreejon Das et al., 2017; UNESCO and HELCOM, 2017). To the best of our knowledge, despite its frequent environmental occurrence, there is no information about the maprotiline environmental fate, its degradation pathway neither toxicity of its degradation products.

This study aims at investigating for the first time the maprotiline environmental fate in river water by initially performing a laboratory simulation to identify the degradation products by HPLC-HRMS and then search for them under natural conditions. For easier identification of the degradation products, maprotiline degradation experiments were firstly performed at high concentration in ultrapure water using $TiO_2$ as a benchmark photocatalyst. Subsequently, experiments were performed in spiked river water, at concentration similar to those described in natural waters, for the elucidation of the drug environmental fate. Toxicity was estimated as well and preliminary bioassays were performed on the generated degradation species.

## 2. Materials and methods

### 2.1. Chemicals

Maprotiline hydrochloride (CAS: 10347-81-6), whose structure with the numbering of carbons atoms is shown in Fig. 1, was purchased from Sigma-Aldrich (Milan, Italy). In order to avoid possible interference from ions adsorbed on the photocatalyst, $TiO_2$ (Evonik P25, Frankfurt, Germany) was irradiated and washed with distilled water, until there were no detectable signals due to chloride, sulfate and sodium ions. All the chemical reagents were used as received. Suspensions and standard solutions were prepared in ultrapure water.

The river water sample was collected from the River Po, Torino Italy, (45°02′40.4″N 7°41′02.1″E) on September 30$^{th}$ 2019. Samples were used after a rough pre-filtration step, carried out through a grade qualitative filter paper (Whatman) removing large suspended solids and filtered using a hydrophilic 0.45 μm filter Sartolon Polyamide (Sartorius Biolab). River water samples had 1.83 mg $L^{-1}$ of total organic carbon (TOC), 44.81 mg $L^{-1}$ of inorganic carbon (IC), and 3.85 mg $L^{-1}$ of total nitrogen (TN) and pH = 8.2. The potential presence of Maprotiline, identified TPs and the described metabolites in the explored river water sample were investigated by HPLC-HRMS before spiking and they were below the detection limit.

### 2.2. Methods

#### 2.2.1. Degradation experiments

The workflow for the maprotiline degradation pathway study is presented in Scheme S1. Maprotiline photocatalytic degradation was carried out in ultrapure water in Pyrex glass cells (2.3 cm height × 4.0 cm diameter), filled with 5 mL of maprotiline (20 mg $L^{-1}$) and $TiO_2$ (500 mg $L^{-1}$) suspension kept under magnetic stirring under irradiation for times ranging from 1 min to 60 min. After irradiation, the photocatalyst was removed using a 0.45 μm Sartolon Polyamide (Sartorius Biolab) filter before analysis. The photolysis experiments were performed in the same conditions without the catalyst addition.

Photolysis experiments in river water sample were performed on a 200 mL water volume spiked with 10 μg $L^{-1}$ of maprotiline divided into three Pyrex glass cells (7.5 cm height × 9.5 cm diameter). Samples were irradiated for times ranging from 1 h to 72 h. The irradiation was carried out using a PHILIPS cleo 6 X 15 W TL-D Actinic BL with

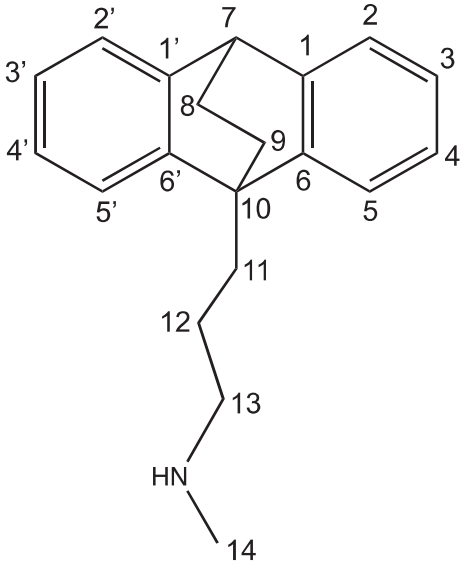



**Fig. 1.** Numbering of maprotiline carbon atoms.

maximum emission wavelength at 365 nm. The UV integrated irradiance on the cells in the 290–400 nm wavelength range was 90 ± 2 $Wm^{-2}$ (measured with a CO.FO.MEGRA (Milan, Italy) power-meter). To control the effect of water sample constituents on maprotiline fate, spiked water samples (10 μg $L^{-1}$) were kept in the dark collecting samples over time (0, 16, 24, 48 and 72 h). Samples were then freeze-dried (LABOGENE – CoolSafe 55-110). The obtained powder was dissolved into 10 mL of a 50:50 (v/v) methanol: acetonitrile mixture which was filtered with a 0.22 μm polypropylene filter (ThermoFisher Scientific). The sample was dried under a gentle nitrogen stream at room temperature, then reconstituted with 200 μL of acetonitrile (final preconcentration factor of 1000) for the LC-HR-MS analysis.

*2.2.2. Analytical procedures*

The identification of maprotiline TPs in ultrapure water and in river water samples was performed using an Ultimate 3000 High Pressure Liquid Chromatography coupled with a LTQ-orbitrap mass spectrometer (Thermo Scientific, Bremen, Germany) operated in ESI mode. The chromatographic separation was achieved with a reverse phase C18 column (Gemini NX C18, 150 × 2 mm, 3 μm, 110 Å; Phenomenex, Castel Maggiore, BO, Italy) using 20 mM aqueous formic acid (eluent A) and acetonitrile (eluent B). Gradient separation ramp started with 5% B, increased up to 40% B in 18 min and to 100% in 5 min; then the column was reconditioned. The flow was 0.2 mL/min and injection volume 20 μL.

For the ESI ion source used nitrogen as both sheath and auxiliary gas. Source parameters were set as followed: sheath gas 30 arbitrary unit (arb), auxiliary gas 25 arb, capillary voltage 4.0 kV and capillary temperature 275 °C. Full mass spectra were acquired in positive ion mode on *m/z* range between 50 and 500 Th, with a resolution of 30.000. $MS^n$ spectra were acquired on the range between ion trap cut-off and precursor ion *m/z* values. Accuracy on recorded *m/z* (versus calculated) was ±0.001 Th (without internal calibration).

For the structural elucidation of TPs, collision-induced dissociation (CID) experiments were performed on an Acquity HPLC system (Water Technologies, Guyancourt, France) coupled with a Bruker SolarixXR FT-ICR 9.4 T MS instrument (Bruker Daltonics, Bremen, Germany). For the chromatographic separation, an Agilent Pursuit XRsULTRA C18 (length 50 mm, diameter 2 mm, particle size 2.8 μm) column was used with an Agilent HPLC MetaGuard (Pursuit XRs C18, 3 μm, 2,0 mm) guard column (Agilent Technologies, Les Ulis, France). The flow was set to 0.2 mL/min, the total run time was 22 min with an acquisition time of 15 min. Gradient flow was used with solvent A being water with 0.1% formic acid and solvent B being acetonitrile with 0.1% formic acid. The LC method consisted of holding 95% of solvent A and 5% of solvent B for 3 min, after which a gradient of 9 min was applied, until the ratio of the two solvents reached 50–50%. The ratio of solvent A was promptly decreased to 5% and kept at this ratio until 17.1 min total run time, after it was reset to the initial 95%. After every measurement, 5 min were let for equilibration and washing using the latter solvent ratio. The injection volumes were 2 μL and 10 μL for LC-MS and LC-$MS^n$ experiments, respectively. The autosampler (Water Technologies, Guyancourt, France) was kept at 4 °C for better preservation. Each sample was prepared before analysis by adding 10% volume of a mixture acetonitrile/formic acid (0.1%). Electrospray ionization was used as the ion source in positive mode with a sample flow of 0.2 mL/min. The capillary voltage was 4000 V and the spray shield was set at −500 V. Nitrogen was used as nebulizer gas (1 bar) and drying gas (8 L/min, 250 °C). The detection range was 57.7–1000 *m/z*, in broadband mode, with a data acquisition size of 4 Mpts and a data reduction of noise of 97%. For $MS^2$ experiments, isolation was carried out with a 1 *m/z* window and CID experiments were performed with collision energies of 5, 10, 15 and 20 V. Preliminary in-cell experiments were performed to assess the optimal parameters (isolation window, quadrupole voltage, and collision energy) for the $MS^3$ experiments. The Bruker Data Analysis software was used for data processing.

Total organic carbon (TOC) was measured using a Shimadzu TOC-5000 analyzer (catalytic oxidation on Pt at 680 °C). The calibration was performed using standards of potassium phthalate.

Inorganic ions ($NO_3^-$, $NO_2^-$ and $NH_4^+$) generated during maprotiline degradation were identified by ion chromatography analysis using a Dionex chromatograph equipped with a Dionex 40 ED pump and a Dionex 40 ED conductimetric detector. For nitrate anions, a Dionex Ion Pac AS9-HC 4 × 250 mm column, and Ion Pac ASRS-ULTRA 4 mm conductivity suppressor were used while ammonium cations were analyzed using a Dionex Ion Pac CS12A 4 × 250 mm column, and an Ion Pac CSRS-ULTRA 4 mm conductivity suppressor, using 10 mM $NaHCO_3$ and 4 mM $K_2CO_3$ as eluent at 1 mL/min.

*2.2.3. Retrospective suspected screening*

The retrospective suspected analysis was performed accordingly to the workflow previously described (Alygizakis et al., 2019b). The occurrence of maprotiline and the elucidated TPs were investigated in 130 digitally achieved chromatograms (58 wastewater and 72 river water samples). 34 wastewater samples from the river basins of Germany (Danube, Rhine, Ems, Weser, Elbe, Odra, Meuse, Eider, Trave, Peene) (Freeling et al., 2019) and 24 additional wastewater samples from Danube River basin (12 countries) (Alygizakis et al., 2019a) and surface water samples from Danube, Dniester (Diamanti et al., 2020) and Donets were investigated, as described in Table S5.

*2.2.4. Toxicity*

The acute toxicity of maprotiline and the degradation products issued from maprotiline (20 $mgL^{-1}$) degradation in ultrapure water in the presence of $TiO_2$ (500 $mgL^{-1}$) was evaluated for samples after different irradiation times using a Microtox Model 500 toxicity analyzer (Milan, Italy). The analyses were performed evaluating the bioluminescence inhibition assay in the marine bacterium *Vibrio fischeri* by monitoring changes in the natural emission of the luminescent bacteria. Freeze-dried bacteria, reconstitution solution, diluent (2% NaCl) and an adjustment solution (non-toxic 22% sodium chloride) were obtained from Azur (Milan, Italy). Samples were tested in a medium containing 2% sodium chloride, and the luminescence was recorded after 5, 15 and 30 min of incubation at 15 °C. The luminescence inhibition percentage was determined by comparing with a non-toxic control solution.

## 3. Results and discussion

### 3.1. Chemical selection approach

Maprotiline was selected as a compound of potential interest for further monitoring activities as a result of the application of the NORMAN prioritization scheme. This scheme was designed by NORMAN to deal with less-investigated substances for which knowledge gaps are identified (e.g. insufficient information on the exposure levels and/or adverse effects, or inadequate performance of the analytical methods for their measurement in the environment) (von der Ohe and Dulio, 2013). The concept involves the application of a decision tree which allows the allocation of substances into six main action categories, based on the identified knowledge gaps and actions needed to address them. The priority within each category is then evaluated on the basis of specific occurrence, hazard (e.g. persistence, bioaccumulation, mobility, endocrine disruption potential) and risk indicators.

This workflow, originally designed to work with target monitoring data, is currently exploring the automatic query of non-target screening (NTS) mass spectral information archived in the Digital Sample Freezing Platform (DSFP).

As part of the NORMAN Database System (NDS) ("NORMAN Database System") and its interconnected databases (SusDat database ("NORMAN Substance Database") ECOTOX database ("NORMAN Ecotoxicology Database"), the NORMAN Digital Sample Freezing Platform (DSFP) (Alygizakis et al., 2020) is a virtual platform able to store

an extensive number of raw HRMS data converted into a common (open) format, designed for retrospective screening. Thanks to a set of fully integrated tools NORMAN DSFP can provide reliable qualitative and semi-quantitative data on the occurrence of CECs, can represent the spatial distribution of contaminants and the degree of exceedance of threshold values and in this way support identification and prioritization of CECs frequently detected in environmental samples.

Maprotiline was identified as a compound of potential interest further to a suspect screening test carried out for a list of more than 40,000 substances (present at the time of the study in the SusDat database, 5th September 2019) on 46 composite effluent wastewater samples collected from Danube river basin (August 2017) (Alygizakis et al., 2019a) and from a national wastewater effluent campaign in Germany (May 2018) (Freeling et al., 2019) archived in DSFP. Considering mass accuracy, plausibility of the chromatographic retention time (RT), isotopic pattern fit, number of experimental and predicted fragments, and % similarity of experimental and library spectra as criteria supporting the tentative identification of the suspects, maprotiline was elucidated at level 2A (probable structure by library spectrum match) as compared to other substances for which actions to improve the elucidation of the structure are needed before implementation of further monitoring effort.

In line with the purposes of the prioritization methodology (worst-case scenario approach), the lowest Provisional No Effect Concentration (PNEC) values were used – representing the most conservative ecotoxicological threshold values for the investigated suspect compounds. All PNEC values used in this study were extracted from the NORMAN Ecotoxicology database. In cases where no experimental data on the toxicity of detected substances were available, predicted PNECs (P-PNECs) were derived by QSTR models (Aalizadeh et al., 2017). The substances were ranked based on three indicators: (*i*) Frequency of Appearance (FoA), calculated as percentage of sites where the substance was detected above the limit of detection (LOD); (*ii*) Frequency of PNEC exceedance (FoE), calculated as percentage of sites where the substance was detected above the PNEC, and (*iii*) extent of PNEC exceedance (EoE), calculated as the 95th percentile (MEC95) of the substance's maximum observed concentration at each site divided by the PNEC. No PNEC value based on experimental data was available for maprotiline and therefore a predicted PNEC (P-PNEC) was used. Maprotiline was prioritized and allocated to the group of compounds with "Sufficient frequency of appearance (FoA)", that is FoA (sites with positive detection) ≥ 20%, (67% of the investigated wastewater treatment stations) with 17% of the sites exceeding the predicted PNEC value (0.300 μg $L^{-1}$).

### 3.2. Maprotiline degradation in ultrapure water

The direct photolysis of maprotiline in the considered time window (1 h) is negligible. The most likely reason is the fact that the molecule does not absorb radiations above 280 nm (Suh and Smith, 1986), while the sunlight irradiance below 300 nm is extremely limited (Frank and Klöpffer, 1988). To hasten the degradation process and generate degradation products, the drug degradation was firstly performed at high concentration (for easier identification) in ultrapure water using $TiO_2$ as photocatalyst. Fig. 2 shows the maprotiline degradation in the presence of the heterogeneous photocatalyst activated under UVA irradiation. In the presence of the photocatalyst, the complete maprotiline removal was achieved after only 15 min, while the total organic carbon (TOC) measurements showed more than 85% of the pollutant mineralization in just 30 min under irradiation and >95% after 1 h. This trend is in agreement with the ammonium and nitrate concentrations monitored during the degradation, as shown in Fig. 2. The ammonium ion (73%) release was observed in a significantly higher amount than that of nitrate (15%) within 1 h of irradiation, as previously observed (Low et al., 1991).

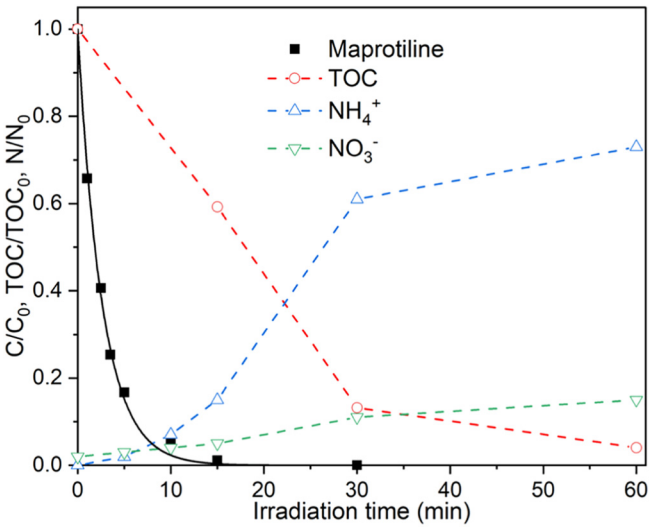



**Fig. 2.** Maprotiline degradation (black line) and mineralization (colored lines) in the presence of $TiO_2$ (500 $mgL^{-1}$).

All samples were analyzed by HPLC-HRMS for the identification of maprotiline degradation products. The *m/z* ratios, proposed elemental compositions, as well as fragment ions and retention times are presented in Table S1 (see supplementary information). In total, 32 degradation products were formed, many of them in the form of several isomeric species as summarized in Table S1. The formation of degradation products and their evolution over irradiation time are shown in Fig. S1. For all degradation products, complete removal was observed after less than 30 min of irradiation, in agreement with the high percentage of mineralization (86%) obtained within the same experimental time.

Among the identified TPs, 18 resulted from the drug hydroxylation. Species with *m/z* 294.1858, 310.1806, 326.1755 and 342.1709 matches with formulae corresponding to mono-, di, tri- and tetrahydroxy derivative isomers. The main drug degradation products were those involving monohydroxylation (*m/z* 294, see Fig. S2), and in particular the isomers 294-D and 294-E, which exhibited maximum intensity within 5 min, as shown in Fig. S1. The species resulting from the addition of the second (*m/z* 310), third (*m/z* 326) and fourth (*m/z* 342) hydroxyl groups showed similar evolution profiles over time. Additionally, 9 degradation products resulting from the drug oxidation were identified.

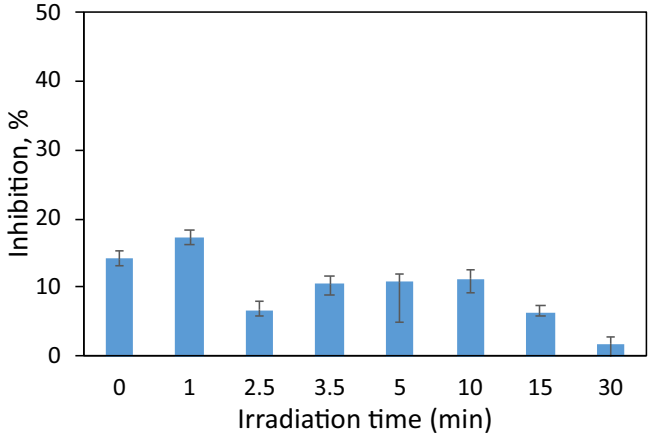



**Fig. 3.** Inhibition effect on Vibrio fischeri bioluminescence in the presence of TPs resulting from maprotiline photocatalytic degradation as a function of irradiation time. Error bars correspond to standard deviations ($n = 3$).

Species with *m/z* 292.1709, 308.1648, 324.1609 match formulae corresponding to dehydrogenation of mono-, di- and trihydroxy derivatives, respectively. It can be reasonably assumed that these TPs are a result of $H_2$ elimination from the corresponding species determined with *m/z* 294, 310 and 326. The TPs with *m/z* 308 showed a fast formation (maximum intensity at 5 min) but a longer persistence, nevertheless they were also completely removed within 30 min. A similar evolution over time was observed for the 3 isomeric species with *m/z* 284.1647 matching with the formula $C_{18}H_{22}NO_2^+$. Additionally, two species at *m/z* 258.1503 and 234.1505 ions were observed, matching respectively with the formulae $C_{16}H_{20}NO_2^+$ and $C_{14}H_{20}NO_2^+$, and both species presented the maximum intensity at 5 min and complete disappearance in 30 min. Furthermore, it could be noted a progressively lower abundance of TPs formed from the addition of multiple hydroxyl groups. Also, the species with *m/z* 284.1647, 258.1503 and 234.1505 were the lowest abundant TPs.

The potential acute toxicity of maprotiline and its TPs was assessed by using the *Vibrio fischeri* assay and the results are plotted in Fig. 3. At time zero, the inhibition percentage related to maprotiline is low (12%) and, despite a slight increase in the first stage of degradation, then it decreases, so implying that the drug transformation proceeds through the formation of slightly toxic compounds. The sample at 30 min presents a percentage of inhibition close to zero in agreement with the complete removal of the identified TPs and the almost complete mineralization.

### 3.2.1. Structural elucidation of maprotiline main degradation products

Aiming at TPs structural elucidation, the maprotiline fragmentation pathway was firstly investigated by CID experiments, ascertaining the most likely losses from the protonated molecule. The maprotiline $MH^+$ (*m/z* 278.1910) $MS^2$ fragmentation pathways are presented in Fig. 4 and was suggested based on the 5 observed product ions (see Table S1).

Five photoproducts with *m/z* 294 were detected with retention times between 9.0 and 11.3 min and, based on their empirical formula, were attributed to hydroxylated maprotiline. If one considers that these

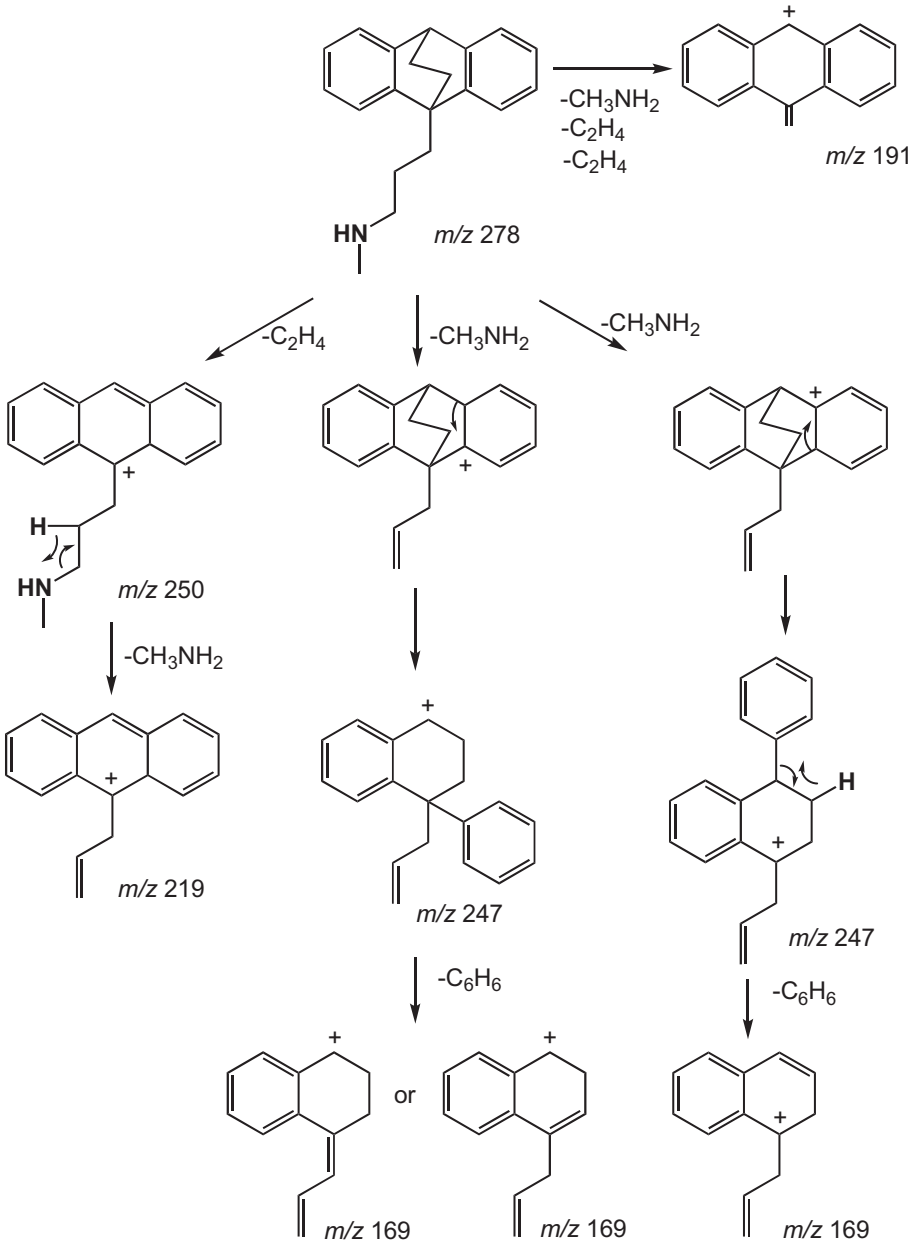



**Fig. 4.** Suggested fragmentation pathways for protonated maprotiline in CID experiments.

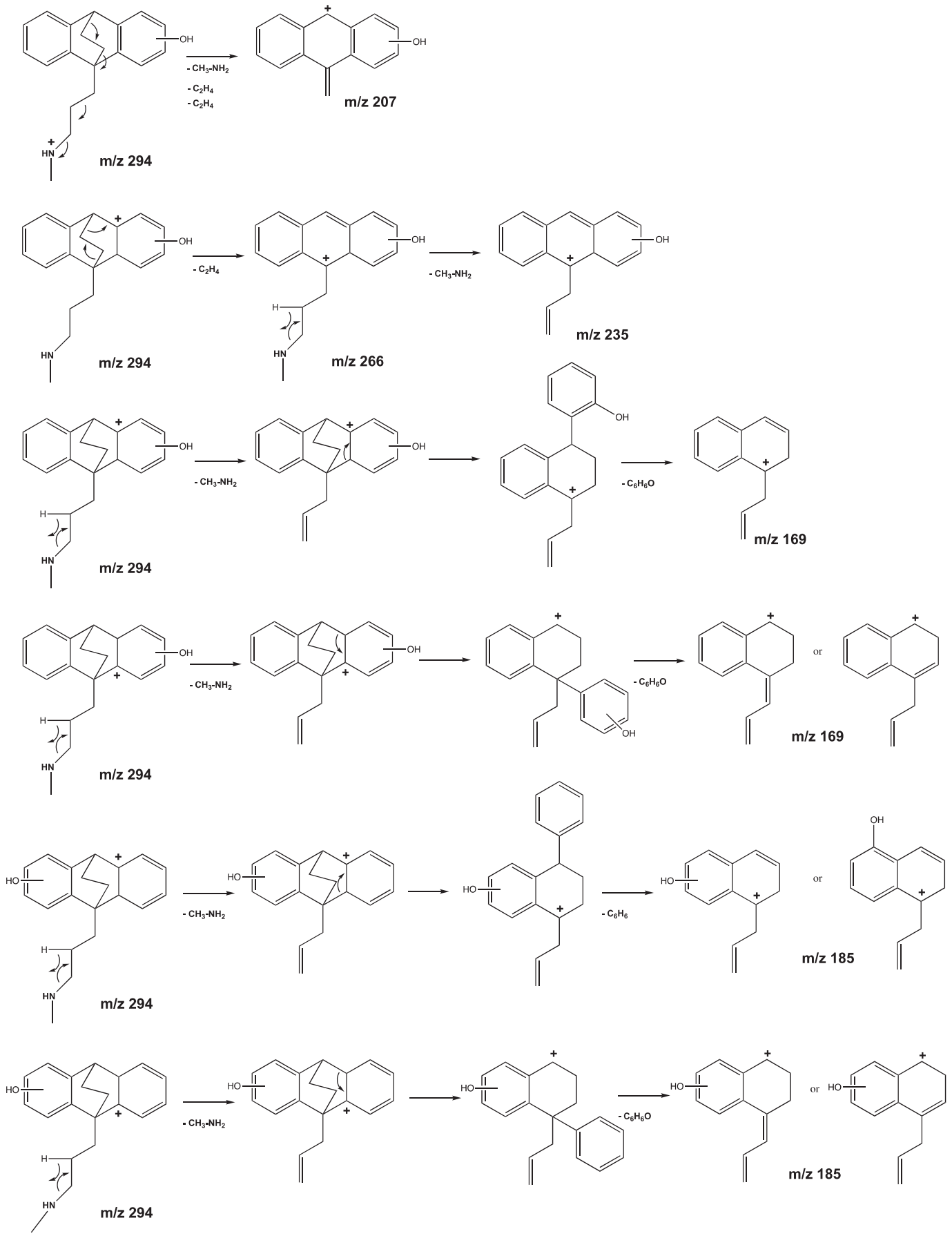



**Fig. 5.** Suggested dissociation pathways for photoproducts resulting from hydroxylation of maprotiline on an aromatic ring.

photoproducts result from hydroxyl addition onto an aromatic ring, as usually reported when photochemistry occurs in water matrix, the main dissociations of oxidized maprotiline are expected to be those displayed in Fig. 5. It is to be noted that water loss from the protonated molecule is not informative considering that protonation of a hydroxyl group can lead to water elimination whatever its location on the ion (Nicolescu, 2017).

The main ions observed in CID experiments on *m/z* 294 are those described in Fig. 5, and are common for the photoproducts 294-A, 294-C, 294-D and 294-E (see Table 1) but not for 294-B, for which CID decomposition pathways are different. The protonated structure of the compound 294-D displays specific ions (*m/z* 263 and *m/z* 245), which allow to determine the position of the hydroxyl group according to the mechanism displayed in Fig. S2. In the same way, the specific ion at *m/z* 157 allowed structural determination of the compound 294-E (see Fig. S4). The CID mass spectra of the photoproducts 294-A and 294-C are the same and do not allow to discriminate between the compound resulting from hydroxyl addition on the carbon atom 3 or onto the carbon atom 4 (see Fig. 1). The structures were suggested based on their relative retention times, in comparison with those of the elucidated structures. In the case of the photoproduct 294-B, CID experiments provided common ions with those resulting from CID of protonated maprotiline: *m/z* 276, *m/z* 250, *m/z* 219 and *m/z* 191, which show evidence that hydroxylation of this compound occurred on the bridge, i.e. on C8 or C9. The CID pathways depicted in Fig. S5 demonstrate that it is not possible to establish whether the hydroxylation took place on carbon 8 or 9 since the CID mechanism begins by a water elimination that leads to the same ion in both cases. One should have expected hydroxylation to occur onto C7 because cleavage of the C7—H bond would have led to a very stable carbocation but the resulting compound would not have been able to undergo the subsequent losses of $H_2O$ and $C_2H_2$ reported in Table 1 for the corresponding ion. Additional experiments (see below) allowed to establish that hydroxylation took place on C9.

Five photoproducts with a pseudo molecular ion at *m/z* 292 were detected with retention times between 9.4 and 11.6 min; in terms of molecular formulae, they result from the addition of one oxygen atom and the removal of two hydrogen atoms on maprotiline. It can be reasonably assumed that these five photoproducts result from $H_2$ elimination from the five photoproducts with a pseudo molecular ion at *m/z* 294. Dehydrogenation is possible to create a double bond between C7 and C8 or C8 and C9, the first hypothesis leading to a more stable species regarding mesomeric effects. This is confirmed by CID mechanisms. Considering for example the molecule 292-B, the formation of ions at *m/z* 250 and *m/z* 119 from $MH^+$ is only possible if the new double bond created is located between C7 and C8 (see Fig. S6). Based on these considerations, the four ions at *m/z* 292 that dissociate to provide ions at *m/z* 250, *m/z* 243, *m/z* 219 and *m/z* 191 were assumed to result from the formation of a double bond between carbon atoms C7 and C8 from the photoproducts with $MH^+$ ions at *m/z* 294. The photoproduct 292-E displays a different CID pathway with product ions at *m/z* 246 and *m/z* 183, which show that in this case the double bond was created on the alkyl chain. It has been assumed to be formed between C12 and C13 because: *i)* it is thus conjugated with the free doublet of the nitrogen atom, *ii)* this localization allows the $C_2H_4$ elimination depicted in Fig. S7. Localization of the hydroxyl group on C9 permits to explain the same mechanism. This last conclusion allowed assigning the structure of the compound 294-B as displayed in Fig. S8 (see supplementary material).

Considering the molecular symmetry of maprotiline and the fact that water loss induced by CID does not allow to attribute the exact position of the corresponding hydroxyl group, it was not always possible to accurately elucidate the structures of the poly hydroxylated species. However, it is reasonable to assume that the second, third and fourth consequent hydroxylations took place on the aromatic ring or the ethylene bridge of species with molecular ions at *m/z* 294 and 292.

Six products with $MH^+$ at *m/z* 310 resulting from the dihydroxylation of maprotiline were detected between 8.4 and 11.3 min. As suggested above, it can be expected that these substances resulted from the hydroxyl addition to the generated monohydroxylated species *m/z* 294. Table S3 summarizes the common ions observed in CID experiments of different isomers and the main dissociation pathways are shown in Fig. S9. In the case of the photoproduct 310-F, CID experiments provided common ions with those resulting from CID of protonated maprotiline: *m/z* 250 and *m/z* 191, which show evidence that hydroxylation of this compound occurred on the bridge, i.e. on C9 and C8 (Fig. S10). The CID experiments of the photoproduct 310-E provided the ions *m/z* 280 and 101, allowing to postulate the hydroxyl group addition in the C2 and C5 (Fig. S11). As evidenced in Fig. S1, this was the most abundant dihydroxylated compound, what can be explained the probability of the second hydroxyl group addition in the

**Table 1**
Ions detected in CID experiments for maprotiline main degradation products.

| *m/z* | Ion formula | 294 | | | | |
|---|---|---|---|---|---|---|
| | | A | B | C | D | E |
| 294.1852 | $C_{20}H_{24}NO^+$ | + | | + | + | + |
| 276.1747 | $C_{20}H_{22}N^+$ | + | + | | + | |
| 266.1539 | $C_{18}H_{20}NO^+$ | + | | + | + | + |
| 263.1447 | $C_{19}H_{19}O^+$ | | | | + | |
| 250.1606[a] | $C_{18}H_{20}N^+$ | | + | | | |
| 245.1341 | $C_{19}H_{17}^+$ | | + | | + | |
| 235.1132 | $C_{15}H_{15}O^+$ | + | | + | + | + |
| 219.1182[a] | $C_{17}H_{15}^+$ | | + | | | |
| 207.0804 | $C_{15}H_{11}O^+$ | + | | + | + | + |
| 191.0868[a] | $C_{15}H_{11}^+$ | | + | | | |
| 185.0973 | $C_{13}H_{13O}^+$ | + | | + | + | + |
| 169.1023[a] | $C_{13}H_{13}^+$ | + | | + | + | + |
| 157.0658 | $C_{11}H_9O^+$ | | | | | + |
| *m/z* | Ion formula | 292 | | | | |
| | | A | B | C | D | E |
| 292.1713 | $C_{20}H_{24}NO^+$ | + | + | + | + | + |
| 250.1605[a] | $C_{18}H_{20}N^+$ | + | + | + | + | |
| 246.1292 | $C_{18}H_{16}N^+$ | | | | | + |
| 243.1183 | $C_{15}H_{15}O^+$ | | | + | + | |
| 219.1182[a] | $C_{17}H_{15}^+$ | + | + | + | + | |
| 217.1025 | $C_{15}H_{11}O^+$ | + | + | + | + | |
| 191.0867[a] | $C_{15}H_{11}^+$ | + | + | + | + | |
| 183.0816 | $C_{13}H_{13O}^+$ | | | | | + |

[a] Product ions observed also in the maprotiline fragmentation.

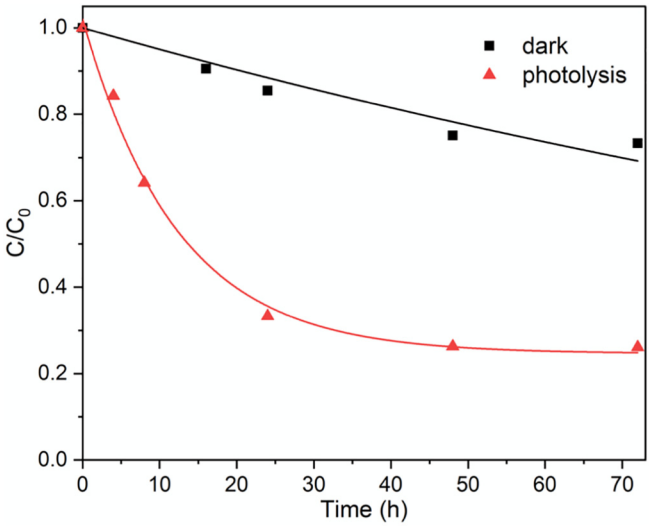



**Fig. 6.** Maprotiline (10 $\mu gL^{-1}$) removal over time in a river water sample, in the dark and under UVA irradiation.

most abundant photoproducts, also formed from the hydroxylation in the C2 (294-E) and C5 (294-D), besides the ortho/para director effect. However, this structure could not be demonstrated due to the lack of product ions. The CID experiments of 310-A, 310-C and 310-D do not permit to elucidate the structure of the isomer. However, the generated ion at *m/z* 251 from 310-C and 310-D species allowed to confirm that the hydroxylation does not occurred on the bridge, i.e. on C8 and C9, while the ion *m/z* 201 from 310-D endorsed to ascertain the dihydroxylation in the same aromatic ring (Fig. S9). The ion *m/z* 266 obtained from CID experiments of compound 310-B evidenced the hydroxyl addition to the bridge, i.e. on C9 if considering this species to result from the hydroxyl group addition to the 294-B. The formation of ions *m/z* 123 and 89 allowed to postulate the hydroxyl group addition on C11, as suggested in Fig. S12. However, the formed ions do not allow demonstrating the suggested structure.

Additionally, three compounds with $MH^+$ at *m/z* 284 were detected with retention times between 8.0 and 9.5 min; they result from ethylene loss and hydroxylation with ring-opening. In the case of 284-A, CID experiments lead to the formation of the fragment at *m/z* 225 through consecutive losses of methylamine and carbon monoxide. The compound 284-C generated the product ion at *m/z* 256 from the loss of ethylene bridge and at *m/z* 225 through the loss of methylamine. The structures were postulated based on these eliminations (Figs. S13 and S14) but the lack of other product ions does not allow their conclusive elucidation. The 284-B generated a single ion at *m/z* 89, allowing speculating the oxygen addition on C3 and C4 with the loss of the ethylene bridge, as proposed in Fig. S15.

A compound with $MH^+$ at *m/z* 258 ($C_{16}H_{20}NO_2^+$) elutes at 7.3 min. The fact that no other isobaric species are detected suggests that it does not result from further oxidation of one the aforementioned hydroxylated species. Only two product ions are detected in CID experiments and correspond to subsequent losses of water and carbon monoxide, which is typical of protonated carboxylic acids. That is why the structure displayed in Fig. S16 is that of a carboxylic acid. Opening of an aromatic ring with the formation of a carboxylic acid is quite frequent in photochemistry (Horspool et al., 2003). Unfortunately, the structure postulated in Fig. S16 was not demonstrated due to the lack of product ions in CID experiments; although its high polarity is in agreement with relatively short retention time.

### 3.3. Simulated and real environmental conditions

The environmental fate of the drug was investigated in natural river water by searching for the TPs detected in the photocatalytic simulation, but also for potential new TPs not observed before. For such, a river water sample was spiked with maprotiline (10 μg $L^{-1}$) at a concentration similar to those previously reported in the environment (UNESCO and HELCOM, 2017). It should be pointed out that, as detailed in Section 2.2.1, the samples were pre-concentrated by freeze-drying before analysis. During degradation experiments, the pH value was measured and compared the initial pH with that measured at the end of the degradation no significant change over time was observed (ΔpH ≤ 0.1).

As evidenced in Fig. 6, experiments performed in the dark showed around 20% of maprotiline removal within 72 h, so implying a limited effect of the biotic components on drug fate. In the dark, the drug degradation leads to the formation of the byproducts 294-D and 284-C, observed after 24 h and 16 h, respectively, and still present after 72 h, as

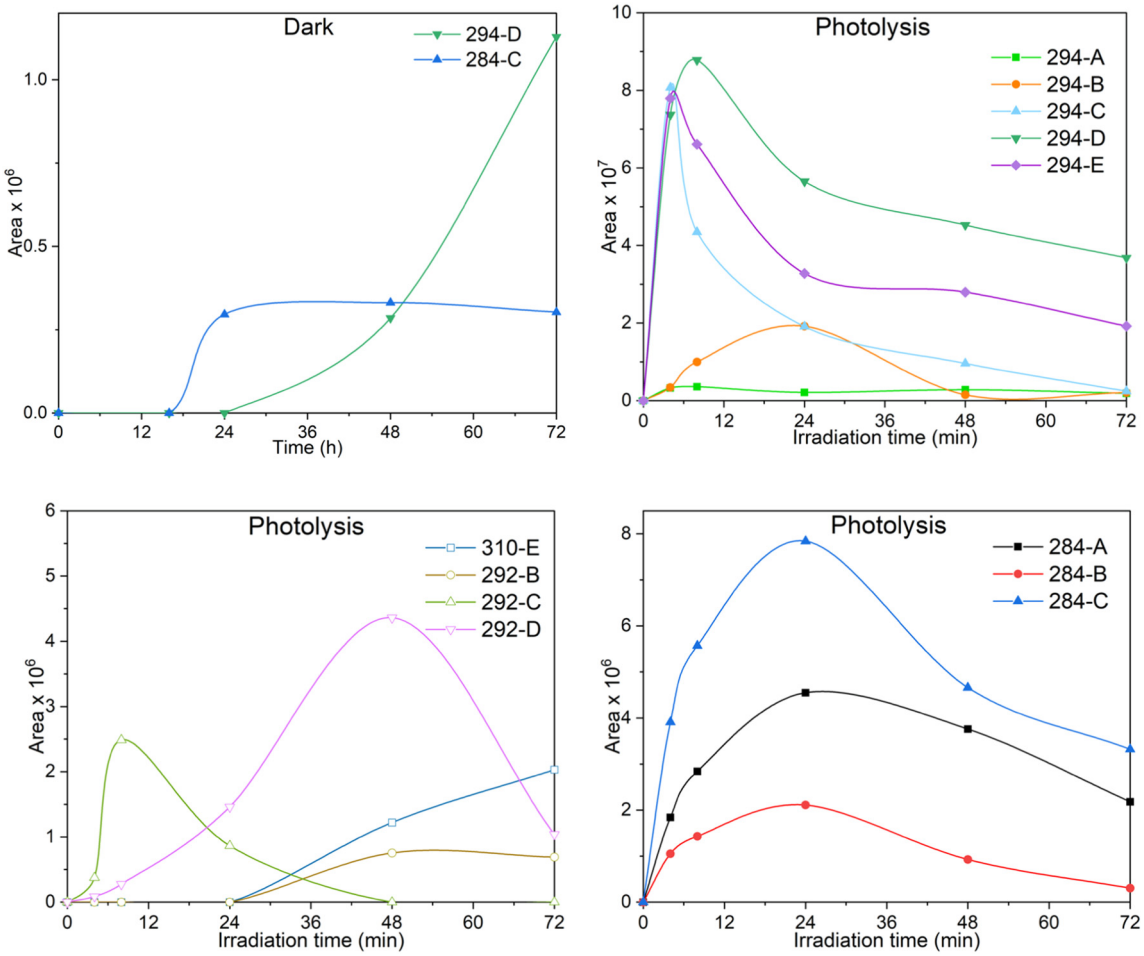



**Fig. 7.** Profile over time of maprotiline degradation products observed in a river water sample over time: a) in the dark; b, c and d) under irradiation.

shown in Fig. 7a. The monohydroxylated species matches with one of the most abundant TPs observed in ultrapure water, while the species with *m/z* 284, was previously observed in low abundance.

Under irradiation, the maprotiline degradation kinetic increased following a pseudo first-order decay until 24 h, achieving 65% of drug removal (Fig. 6), while the appearance of TPs is also favored compared to dark conditions. In detail, 12 out of the 32 TPs previously identified (see Table S4) were found in spiked river water and all were still present after 72 h irradiation. All the 5 isomeric forms of the monohydroxylated species ($MH^+$ at *m/z* 294) were observed, 294-C, 294-D and 294-E in significantly larger amounts (Fig. 7). It is interesting to note the slower formation of 294-B, the only isomer resulting from hydroxylation on the bridge and not on an aromatic ring (see Section 3.2.1). From the literature, it is possible to realize that besides maprotiline degradation, the species 294-A (2-hydroxymaprotiline) and 294-C (3-hydroxymaprotiline) can reach the environment also from drug metabolization; hydroxylated products represent 4–8% of the dose being excreted in human urine, with 3-hydroxymaprotiline and the corresponding *N*-demethylated specie reported as major human metabolites (Breyer-Pfaff et al., 1985). Additionally, the study identifies metabolites resulting from hydroxylation on the C8 atom (ethylene bridge) and the corresponding demethylation product, besides the metabolite resulted from the di-hydroxylation in C3 and C4.

The species 292-B, 292-C and 292-D, issued from dehydrogenation of the most abundant 294 isomers, (with the formation of a double bond between atoms C7 and C8, see Section 3.1.1) show distinct evolutions over time. 292-C showed its maximum intensity at 4 h and was completely removed within 48 h, 292-D reached its maximum intensity at 48 h and was still present at 72 h, while 292-B appeared after 24 h and decreased until the end of the experiment.

Only one specie formed by the addition of more than one hydroxyl group was detected. Resulting from the addition of two hydroxyl groups, the compound 310-E was formed after 24 h irradiation with increasing abundance until the end of the experiment. As stated before (see Section 3.1.1) this compound was the most abundant dihydroxylated observed in photocatalytic experiments in ultrapure water and resulted from a second hydroxyl group addition into the most abundant monohydroxylated species (294-D and 294-E).

Additionally, the 3 species at *m/z* 284 resulting from the ring-opening were also formed with maximum intensity at 24 h, showing a slow degradation profile and still present at the end of the experiment. One could argue that the species $MH^+$ at *m/z* 284 resulted from the degradation through ring-opening of the dihydroxylated compounds ($MH^+$ at *m/z* 310), particularly the 284-A resulting from the degradation of the compound 310-E. However, as evidenced in Fig. 7, the species $MH^+$ at *m/z* 284 are formed at the early steps of maprotiline degradation, while the compound 310-E was observed only after 24 h, so implying that ring-opening pathway occurs from maprotiline molecule. Fig. 8 displays the proposed maprotiline degradation pathways in river water.

All the TPs observed in river water experiments matched with those previously identified in the photocatalytic experiments performed in ultrapure water, as previously observed for other pollutants (Katagi, 2018; Sirtori et al., 2010).

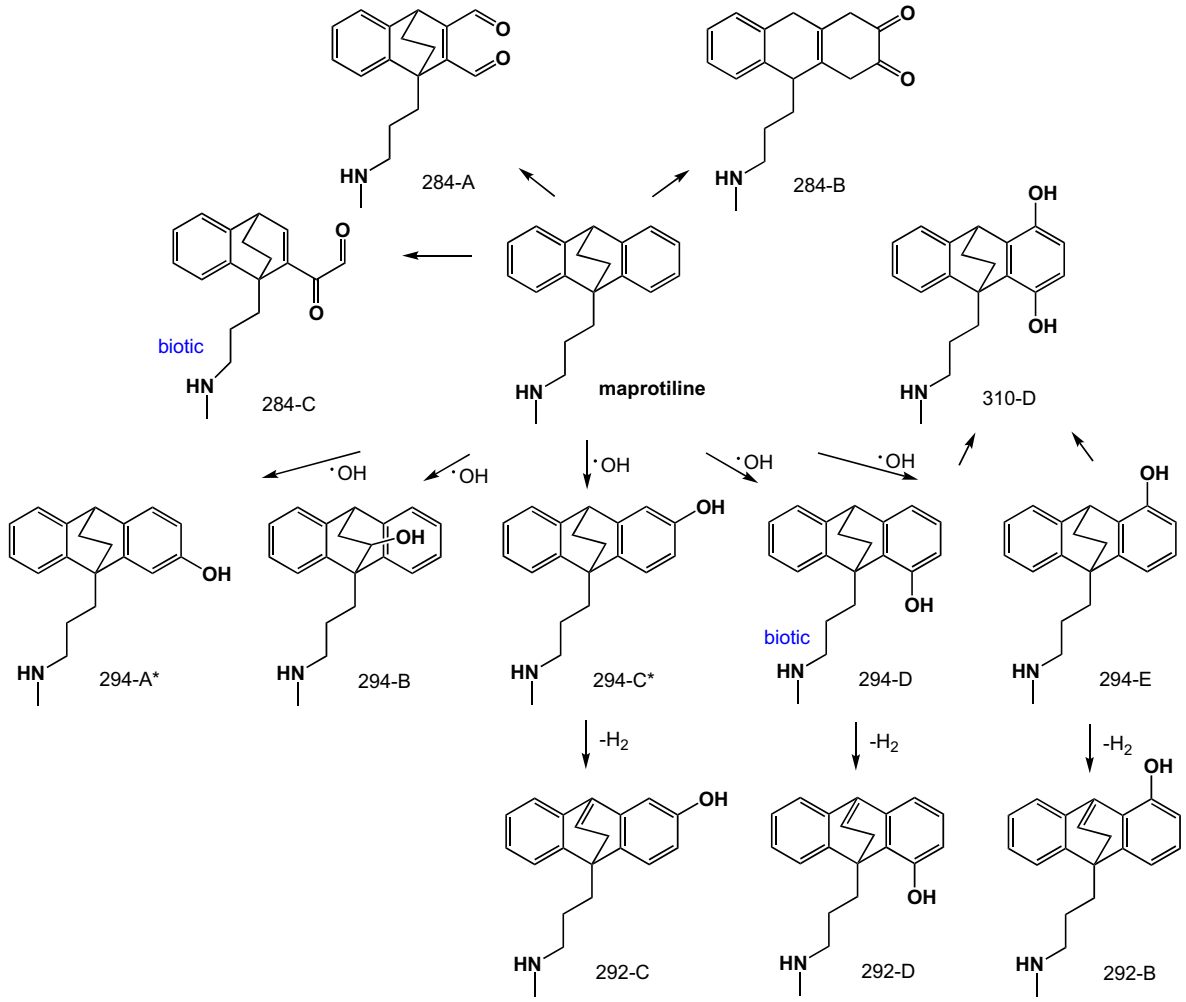



**Fig. 8.** Proposed maprotiline degradation pathways in river water in the dark (biotic) and under irradiation (abiotic) *indicated TPs also resulted from human metabolic transformation.

Additionally, the faster photodegradation rate observed in river water experiments relative to the degradation in ultrapure water indicated that indirect photolysis played an important role in the drug removal. Faster photodegradation of organic pollutants in wastewater has been reported by other authors (Dong et al., 2015; Rering et al., 2017; Wang et al., 2017), while nitrate and dissolved organic matter have been identified as photosensitizers responsible for the generation of reactive species (Bodhipaksha et al., 2017; Dong et al., 2015; Minero et al., 2007).

The results of the retrospective suspect screening presented in Table S4 indicate that the elucidated TPs by laboratory-scale experiments are formed in real waters. 16 TPs were detected in at least one effluent wastewater sample with maprotiline 308-B showing the highest frequency of appearance (FoA 56.9%). This fact creates concerns about the toxicity of the formed chemical mixture in wastewaters. Despite the formation and the detection of numerous TPs in real wastewater, most of the TPs remained undetectable in river water samples. Maprotiline and three TPs (308-B, 326-C, Maprotiline 234) were the only TPs that were scarcely detected in river waters (FoA below 2.8%), which indicates that the substance is further degraded in the environment and the concentration of the substance and its TPs becomes lower than the limit of the detection of the applied sample preparation and instrumental methods.

## 4. Conclusions

The degradation of maprotiline in spiked river water led to the formation of twelve TPs, structurally elucidated through LC/HR-MS. The degradation pathways in natural water were proposed for the first time, which results from monohydroxylation in several positional isomers and the corresponding dehydrogenated molecules, besides dihydroxylation and ring-opening. Some of these TPs, 2-hydroxymaprotiline and 3-hydroxymaprotiline matched with described maprotiline metabolites, that can be released in the environment by drug excretion.

Moreover, photocatalytic experiments led to the formation of a higher number of TPs, mostly resulting from similar chemical transformation in multiple positions.

Additionally, retrospective suspect screening of wastewater effluents and river water samples indicate that the elucidated TPs by laboratory-scale experiments are formed in real waters.

*Vibrio fischeri* Microtox assay allowed estimating that maprotiline photocatalytic degradation leads to the formation of slightly more toxic TPs than the parent compound. Therefore, future research should focus on evaluating the toxicity of the formed TPs in wastewater treatment plants.

## CRediT authorship contribution statement

**Nuno P.F. Gonçalves:** Investigation, Writing - original draft, Writing - review & editing. **Zsuzsanna Varga:** Investigation, Software. **Stéphane Bouchonnet:** Methodology, Validation. **Valeria Dulio:** Conceptualization, Formal analysis. **Nikiforos Alygizakis:** Writing - review & editing, Formal analysis. **Federica Dal Bello:** Data curation, Formal analysis. **Claudio Medana:** Methodology, Validation. **Paola Calza:** Conceptualization, Methodology, Funding acquisition.

## Declaration of competing interest

The authors declare that they have no known competing financial interests or personal relationships that could have appeared to influence the work reported in this paper.

## Acknowledgements

This work is part of a project that has received funding from the European Union's Horizon 2020 - Research and Innovation Framework Programme under the Marie Skłodowska-Curie Grant Agreement No 765860 (AQUAlity).

## Appendix A. Supplementary data

Supplementary data to this article can be found online at https://doi.org/10.1016/j.scitotenv.2020.143556.

## References

Aalizadeh, R., von der Ohe, P.C., Thomaidis, N.S., 2017. Prediction of acute toxicity of emerging contaminants on the water flea Daphnia magna by Ant Colony Optimization-Support Vector Machine QSTR models. Environ Sci Process Impacts 19, 438–448. https://doi.org/10.1039/c6em00679e.

Abbing-Karahagopian, V., Huerta, C., Souverein, P.C., De Abajo, F., Leufkens, H.G.M., Slattery, J., Alvarez, Y., Miret, M., Gil, M., Oliva, B., Hesse, U., Requena, G., De Vries, F., Rottenkolber, M., Schmiedl, S., Reynolds, R., Schlienger, R.G., De Groot, M.C.H., Klungel, O.H., Van Staa, T.P., Van Dijk, L., Egberts, A.C.G., Gardarsdottir, H., De Bruin, M.L., 2014. Antidepressant prescribing in five European countries: application of common definitions to assess the prevalence, clinical observations, and methodological implications. Eur. J. Clin. Pharmacol. 70, 849–857. https://doi.org/10.1007/s00228-014-1676-z.

Alygizakis, N.A., Besselink, H., Paulus, G.K., Oswald, P., Hornstra, L.M., Oswaldova, M., Medema, G., Thomaidis, N.S., Behnisch, P.A., Slobodnik, J., 2019a. Characterization of wastewater effluents in the Danube River Basin with chemical screening, in vitro bioassays and antibiotic resistant genes analysis. Environ. Int. 127, 420–429. https://doi.org/10.1016/j.envint.2019.03.060.

Alygizakis, N.A., Oswald, P., Thomaidis, N.S., Schymanski, E.L., Aalizadeh, R., Schulze, T., Oswaldova, M., Slobodnik, J., 2019b. NORMAN digital sample freezing platform: a European virtual platform to exchange liquid chromatography high resolution-mass spectrometry data and screen suspects in "digitally frozen" environmental samples. TrAC - Trends Anal. Chem. 115, 129–137. https://doi.org/10.1016/j.trac.2019.04.008.

Alygizakis, N.A., Urík, J., Beretsou, V.G., Kampouris, I., Galani, A., Oswaldova, M., Berendonk, T., Oswald, P., Thomaidis, N.S., Slobodnik, J., Vrana, B., Fatta-Kassinos, D., 2020. Evaluation of chemical and biological contaminants of emerging concern in treated wastewater intended for agricultural reuse. Environ. Int. 138, 105597. https://doi.org/10.1016/j.envint.2020.105597.

Aronson, J.K., 2016. Meyler's Side Effects of Drugs: The International Encyclopedia of Adverse Drug Reactions and Interactions, 16th Editi. Elsevier Science.

aus der Beek, T., Weber, F.A., Bergmann, A., Hickmann, S., Ebert, I., Hein, A., Küster, A., 2016. Pharmaceuticals in the environment-global occurrences and perspectives. Environ. Toxicol. Chem. 35, 823–835. https://doi.org/10.1002/etc.3339.

Bodhipaksha, L.C., Sharpless, C.M., Chin, Y.P., MacKay, A.A., 2017. Role of effluent organic matter in the photochemical degradation of compounds of wastewater origin. Water Res. 110, 170–179. https://doi.org/10.1016/j.watres.2016.12.016.

Brack, W., Ait-Aissa, S., Altenburger, R., Cousins, I., Dulio, V., Escher, B., Focks, A., Ginebreda, A., Hering, D., Hilscherová, K., Hollender, J., Hollert, H., Kortenkamp, A., de Alda, M.L., Posthuma, L., Schymanski, E., Segner, H., Slobodnik, J., 2019. Let us empower the WFD to prevent risks of chemical pollution in European rivers and lakes. Environ. Sci. Eur. 31, 10–12. https://doi.org/10.1186/s12302-019-0228-7.

Breyer-Pfaff, U., Kroeker, M., Winkler, T., Kriemler, P., 1985. Isolation and identification of hydroxylated maprotiline metabolites. Xenobiotica 15, 57–66. https://doi.org/10.3109/00498258509045335.

Brodin, T., Fick, J., Jonsson, M., Klaminder, J., 2013. Dilute concentrations of a psychiatric drug alter behavior of fish from natural populations. Science (80-.) 339, 814–815. https://doi.org/10.1126/science.1226850.

David, A., Lange, A., Tyler, C.R., Hill, E.M., 2018. Concentrating mixtures of neuroactive pharmaceuticals and altered neurotransmitter levels in the brain of fish exposed to a wastewater effluent. Sci. Total Environ. 621, 782–790. https://doi.org/10.1016/j.scitotenv.2017.11.265.

Diamanti, K.S., Alygizakis, N.A., Nika, M.C., Oswaldova, M., Oswald, P., Thomaidis, N.S., Slobodnik, J., 2020. Assessment of the chemical pollution status of the Dniester River basin by wide-scope target and suspect screening using mass spectrometric techniques. Anal. Bioanal. Chem. 412, 4893–4907. https://doi.org/10.1007/s00216-020-02648-y.

Dong, M.M., Trenholm, R., Rosario-Ortiz, F.L., 2015. Photochemical degradation of atenolol, carbamazepine, meprobamate, phenytoin and primidone in wastewater effluents. J. Hazard. Mater. 282, 216–223. https://doi.org/10.1016/j.jhazmat.2014.04.028.

Ebele, A.J., Abou-Elwafa Abdallah, M., Harrad, S., 2017. Pharmaceuticals and personal care products (PPCPs) in the freshwater aquatic environment. Emerg. Contam. 3, 1–16. https://doi.org/10.1016/j.emcon.2016.12.004.

Ford, A.T., Herrera, H., 2019. 'Prescribing' psychotropic medication to our rivers and estuaries. BJPsych Bull. 43, 147–150. https://doi.org/10.1192/bjb.2018.72.

Frank, R., Klöpffer, W., 1988. Spectral solar photon irradiance in Central Europe and the adjacent North Sea. Chemosphere 17, 985–994. https://doi.org/10.1016/0045-6535(88)90069-0.

Freeling, F., Alygizakis, N.A., von der Ohe, P.C., Slobodnik, J., Oswald, P., Aalizadeh, R., Cirka, L., Thomaidis, N.S., Scheurer, M., 2019. Occurrence and potential environmental risk of surfactants and their transformation products discharged by wastewater treatment plants. Sci. Total Environ. 681, 475–487. https://doi.org/10.1016/j.scitotenv.2019.04.445.

Gogoi, A., Mazumder, P., Kumar, V., Chaminda, G.G.T., Kyoungjin, A., Kumar, M., 2018. Occurrence and fate of emerging contaminants in water environment: a review. Groundw. Sustain. Dev. 6, 169–180. https://doi.org/10.1016/j.gsd.2017.12.009.

Hollender, J., van Bavel, B., Dulio, V., Farmen, E., Furtmann, K., Koschorreck, J., Kunkel, U., Krauss, M., Munthe, J., Schlabach, M., Slobodnik, J., Stroomberg, G., Ternes, T., Thomaidis, N.S., Togola, A., Tornero, V., 2019. High resolution mass spectrometry-based non-target screening can support regulatory environmental monitoring and chemicals management. Environ. Sci. Eur. 31. https://doi.org/10.1186/s12302-019-0225-x.

Horspool, W.M., Lenci, F., Lenci, F., 2003. CRC Handbookof Organic Photochemistry and Photobiology, Volumes 1 & 2, Second Edition, CRC Handbookof Organic Photochemistry and Photobiology. Second edition. Volumes 1 & 2. CRC Press. https://doi.org/10.1201/9780203495902.

Katagi, T., 2018. Direct photolysis mechanism of pesticides in water. J. Pestic. Sci. 43, 57–72. https://doi.org/10.1584/jpestics.D17-081.

Krzeminski, P., Tomei, M.C., Karaolia, P., Langenhoff, A., Almeida, C.M.R., Felis, E., Gritten, F., Andersen, H.R., Fernandes, T., Manaia, C.M., Rizzo, L., Fatta-Kassinos, D., 2019. Performance of secondary wastewater treatment methods for the removal of contaminants of emerging concern implicated in crop uptake and antibiotic resistance spread: a review. Sci. Total Environ. 648, 1052–1081. https://doi.org/10.1016/j.scitotenv.2018.08.130.

Küster, A., Adler, N., 2014. Pharmaceuticals in the environment: scientific evidence of risks and its regulation. Philos. Trans. R. Soc. B Biol. Sci 369. https://doi.org/10.1098/rstb.2013.0587.

Lai, W.W.P., Lin, Y.C., Tung, H.H., Lo, S.L., Lin, A.Y.C., 2016. Occurrence of pharmaceuticals and perfluorinated compounds and evaluation of the availability of reclaimed water in Kinmen. Emerg. Contam. 2, 135–144. https://doi.org/10.1016/j.emcon.2016.05.001.

Loos, R., Carvalho, R., António, D.C., Comero, S., Locoro, G., Tavazzi, S., Paracchini, B., Ghiani, M., Lettieri, T., Blaha, L., Jarosova, B., Voorspoels, S., Servaes, K., Haglund, P., Fick, J., Lindberg, R.H., Schwesig, D., Gawlik, B.M., 2013. EU-wide monitoring survey on emerging polar organic contaminants in wastewater treatment plant effluents. Water Res. 47, 6475–6487. https://doi.org/10.1016/j.watres.2013.08.024.

Low, G.K.C., McEvoy, S.R., Matthews, R.W., 1991. Formation of nitrate and ammonium ions in titanium dioxide mediated photocatalytic degradation of organic compounds containing nitrogen atoms. Environ. Sci. Technol. 25, 460–467. https://doi.org/10.1021/es00015a013.

Minero, C., Chiron, S., Falletti, G., Maurino, V., Pelizzetti, E., Ajassa, R., Carlotti, M.E., Vione, D., 2007. Photochemincal processes involving nitrite in surface water samples. Aquat. Sci. 69, 71–85. https://doi.org/10.1007/s00027-007-0881-6.

Nawaz, T., Sengupta, S., 2018. Chapter 4 - Contaminants of Emerging Concern: Occurrence, Fate, and Remediation, Advances in Water Purification Techniques: Meeting the Needs of Developed and Developing Countries. Elsevier Inc https://doi.org/10.1016/B978-0-12-814790-0.00004-1.

Nicolescu, T.O., 2017. Interpretation of mass spectra. Mass Spectrometry. InTech https://doi.org/10.5772/intechopen.68595.

NORMAN Database System, d. . [WWW document], n.d. URL. https://www.norman-network.com/nds/. (Accessed 30 July 2020).

NORMAN Databases, d. . [WWW document], n.d. URL. https://www.norman-network.net/?q=node/24. (Accessed 11 April 2020).

NORMAN Ecotoxicology Database, d. . [WWW document], n.d. URL. https://www.norman-network.com/nds/ecotox/. (Accessed 30 July 2020).

NORMAN Substance Database, d. . [WWW document], n.d. URL. https://www.norman-network.com/nds/susdat/. (Accessed 30 July 2020).

Pratt, L., Brody, D., Gu, Q., 2017. Antidepressant Use among Persons Aged 12 and Over: United States, 2011–2014. NCHS Data Brief. Number 283. Natl. Cent. Heal. Stat, pp. 2011–2014.

Rering, C., Williams, K., Hengel, M., Tjeerdema, R., 2017. Comparison of direct and indirect photolysis in imazosulfuron photodegradation. J. Agric. Food Chem. 65, 3103–3108. https://doi.org/10.1021/acs.jafc.7b00134.

Sauvé, S., Desrosiers, M., 2014. A review of what is an emerging contaminant. Chem. Cent. J 8, 1–7. https://doi.org/10.1186/1752-153X-8-15.

Sehonova, P., Svobodova, Z., Dolezelova, P., Vosmerova, P., Faggio, C., 2018. Effects of waterborne antidepressants on non-target animals living in the aquatic environment: a review. Sci. Total Environ. 631–632, 789–794. https://doi.org/10.1016/j.scitotenv.2018.03.076.

Sirtori, C., Agüera, A., Gernjak, W., Malato, S., 2010. Effect of water-matrix composition on trimethoprim solar photodegradation kinetics and pathways. Water Res. 44, 2735–2744. https://doi.org/10.1016/j.watres.2010.02.006.

Sreejon Das, Nillohit Mitra Ray, J.W., Adnan Khan, T.C., Ray, M.B., 2017. Micropollutants in wastewater: Fate and removal processes. Physico-Chemical Wastewater Treatment and Resource Recovery, pp. 75–107 https://doi.org/10.5772/57353.

Suh, S.K., Smith, J.B., 1986. Maprotiline hydrochloride. Anal. Profiles Drug Subst. Excipients 15, 393–426. https://doi.org/10.1016/S0099-5428(08)60420-7.

UNESCO, 2019. World Water Assessment Programme (Paris).

UNESCO, HELCOM, 2017. Pharmaceuticals in the Aquatic Environment of the Baltic Sea Region – A Status Report. UNESCO Emerging Pollutants in Water Series – No. 1, Report. UNESCO Publishing, Paris.

Vandermeersch, G., Lourenço, H.M., Alvarez-Muñoz, D., Cunha, S., Diogène, J., Cano-Sancho, G., Sloth, J.J., Kwadijk, C., Barcelo, D., Allegaert, W., Bekaert, K., Fernandes, J.O., Marques, A., Robbens, J., 2015. Environmental contaminants of emerging concern in seafood - European database on contaminant levels. Environ. Res. 143, 29–45. https://doi.org/10.1016/j.envres.2015.06.011.

von der Ohe, P.C., Dulio, V., 2013. NORMAN Prioritisation Framework for Emerging Substances.

Wang, Y., Roddick, F.A., Fan, L., 2017. Direct and indirect photolysis of seven micropollutants in secondary effluent from a wastewater lagoon. Chemosphere 185, 297–308. https://doi.org/10.1016/j.chemosphere.2017.06.122.